NASA TECHNICAL MEMORANDUM

NASA TM X-3508

NASA TM X-3508

EXPERIMENTAL APPARATUS FOR INVESTIGATION OF FAN AEROELASTIC INSTABILITIES IN TURBOMACHINERY

William H. Jones, Walter A. Bishop,
Thomas A. Kirchgessner, and John H. Dicus

Lewis Research Center
Cleveland, Ohio 44135

NATIONAL AERONAUTICS AND SPACE ADMINISTRATION • WASHINGTON, D. C. • JUNE 1977

[redacted]

1. Report No. NASA TM X-3508	2. Government Accession No.	3. Recipient's Catalog No.
4. Title and Subtitle EXPERIMENTAL APPARATUS FOR INVESTIGATION OF FAN AEROELASTIC INSTABILITIES IN TURBOMACHINERY		5. Report Date June 1977
		6. Performing Organization Code
7. Author(s) William H. Jones, Walter A. Bishop, Thomas A. Kirchgessner, and John H. Dicus		8. Performing Organization Report No. E-9088
		10. Work Unit No. 505-05
9. Performing Organization Name and Address Lewis Research Center National Aeronautics and Space Administration Cleveland, Ohio 44135		11. Contract or Grant No.
12. Sponsoring Agency Name and Address National Aeronautics and Space Administration Washington, D.C. 20546		13. Type of Report and Period Covered Technical Memorandum
		14. Sponsoring Agency Code
15. Supplementary Notes		

16. Abstract

An experimental investigation into the nature of aeroelastic instabilities in turbomachinery has been initiated by the Lewis Research Center. This report deals with the experimental apparatus used during one phase of this program - the testing of a turbofan engine in the subsonic stalled flutter mode of the first fan rotor. The report describes the engine installation, the modifications to the engine controls to obtain off-schedule operation of the fan, engine aerodynamic instrumentation, and general data acquisition systems. Of special interest are sections describing the application, installation, and monitoring of dynamic strain-gage instrumentation on the rotating fan blades.

17. Key Words (Suggested by Author(s)) Engine test facilities Flutter testing Strain-gage instrumentation	18. Distribution Statement Unclassified - unlimited STAR Category 07

19. Security Classif. (of this report)	20. Security Classif. (of this page)	21. No. of Pages	22. Price*
Unclassified	Unclassified	31	A03

* For sale by the National Technical Information Service, Springfield, Virginia 22161

EXPERIMENTAL APPARATUS FOR INVESTIGATION OF FAN AEROELASTIC INSTABILITIES IN TURBOMACHINERY

by William H. Jones, Walter A. Bishop, Thomas A. Kirchgessner, and John H. Dicus

Lewis Research Center

SUMMARY

NASA Lewis has begun an experimental investigation into the nature of aeroelastic instabilities in turbomachinery. The experimental apparatus used for one phase of this program, the testing of a turbofan engine in the subsonic stall-flutter mode of the first fan rotor, is the subject of this report. This report describes the engine installation, the modifications to the engine controls to obtain off-schedule operation, the engine aerodynamic instrumentation, and general data acquisition systems. Of special interest are sections describing the installation and use of dynamic strain gages for monitoring structural vibrations associated with flutter. Rotating strain gages were installed on titanium blades using a procedure that incorporated an aluminum oxide base coat and ceramic cement. After some 42 hours of testing, approximately 25 percent of the strain gages installed were still operating satisfactorily. The predominant failure mode was the debonding and breaking of the nickel-ribbon lead wires. The loss of lead-wire continuity resulted in the abandonment of the common ground system for strain-gage data acquisition and led to a separate pair of wires for each strain gage through the slip ring to the signal conditioning amplifiers.

INTRODUCTION

This report describes the apparatus used in the experimental investigation of the characteristics of subsonic stalled flutter in the first fan rotor of a turbofan engine. The problem of aeroelastic instability (often referred to as flutter) in turbomachinery has been noted throughout the history of gas-turbine development. In the past, empirical analysis and cut-and-try fixes have been used to solve the problem. The trend in modern engine design to increase engine pressure ratio for greater efficiency and to use thinner airfoil sections (consistent with transonic design) to reduce compressor size and weight has led to a shift in structural and aerodynamic loading, which has increased the likelihood of flutter. It is necessary, therefore, to understand the causes and the methods of avoiding the various types of aeroelastic instabilities. To date, few major investigations on full-scale engines have been conducted or reported in the literature. In consideration of this, NASA has begun an experimental and analytic investigation of fan and compressor aeroelastic instability in order to provide both a substantial data base for experimental analysis and a consistent analytic model.

This report presents information on a number of topics relative to experimental flutter testing, such as engine control modifications to achieve off-schedule engine operations, high-response aerodynamic instrumentation, and general data acquisition. Also reported are the particulars of the dynamic strain-gage instrumentation required to provide a reasonably complete picture of blade vibrations. Reference 1 summarizes the data obtained from the experimental program and provides preliminary data reduction and analysis.

ENGINE INSTALLATION, CONTROLS, AND MODIFICATIONS

General

The engine was installed in one of the altitude test facilities at Lewis (fig. 1). The facility provides control of engine inlet and exhaust air (pressure and temperature of the inlet and pressure of the exhaust), some control of the test-cell environment by means of the bulkhead valve (fig. 1), and a cooling-air system (not shown in the fig.). A labyrinth seal was provided at the inlet duct-bulkhead interface to restrain static and dynamic interactions between the engine and the test facility and to allow for measurement of engine thrust. (The engine thrust stand was locked and not used during the test.) A rubber boot seal was also placed between the engine and the inlet duct to provide further structural isolation. Engine inlet details are provided in figure 2.

Exhaust Nozzle Plug

During the course of flutter testing, the exhaust nozzle had to be closed to a smaller than normal area (i.e., the standard minimum mechanical area) in order to raise fan pressure ratios above the normal operating line and thereby locate regions of flutter. An exhaust nozzle plug was installed on the exhaust collector, with the constant area section of the plug extending into the engine nozzle 44.45 centimeters (17.5 in.) aft of station 8. It was experimentally determined that this configuration would not permit proper operation of the pressure-balanced nozzle and that even normal scheduled exhaust areas could not be achieved. Further, it was noted that, at the minimum achievable area condition, considerable distortion of the exhaust nozzle leaves was occurring. The shallow penetration of the plug into the nozzle caused adverse pressure distributions to form inside the nozzle, thus overpowering the actuators and causing distortion of the nozzle leaves.

The plug was reconfigured to increase the penetration of the plug to bring the front of the constant-area section of the plug to 19.05 centimeters ahead of station 8 (see fig. 3). Later testing demonstrated that this configuration allowed full and effective control of the exhaust nozzle into the desired regions.

Compressor Inlet Variable Vanes and Exhaust Nozzle Controls

The search for and the mapping of flutter regions in the fan required controlled, off-schedule operation of the engine. It was determined that this operation could be accomplished by independent control of the fan inlet guide vanes (referred to herein as the compressor-inlet variable vanes (CIVV)) and the exhaust nozzle. (The exhaust nozzle and its attendant primary area are denoted herein as A_8.) Accordingly, the engine systems for commanding actuation of these devices were disabled, and alternative command systems installed as detailed in figures 4 and 5.

Both actuator systems employ hydraulic actuating pistons (with electric feedback units), which are connected to the existing actuating linkages on the engine. The hydraulic flow to the pistons was controlled by electrohydraulic servovalves with fail-safe capabilities for both electric and/or hydraulic power supply failure. The fail-safe position for the CIVV is the fully cambered position. The fail-safe for the exhaust nozzle takes no actions, and the nozzle remains at the setting in effect at the time of failure. The choice for the CIVV fail-safe position was based on the fact that the fully cambered position gives the greatest amount of inlet preswirl. This reduces the first rotor incidence angle to a minimum, thus giving the greatest margin of safety for stalled (positive incidence) flutter in the fan first-stage rotor. Stalled flutter was believed to be the critical form of flutter in the fan of this engine. The A_8 fail-safe condition was chosen to avoid inadvertent repositioning of the nozzle, which could result (in some off-schedule operations) in a stall/surge, overspeed, or choke condition, depending on what type of flutter was being investigated at the time of failure.

Electric control for the electrohydraulic actuator valves can be provided by any of several devices. Selection is made via switches in the control room (figs. 4 and 5). The CIVV is controlled by a analog computer controller (to duplicate standard engine schedules) and, alternatively, by a manual potentiometer (for off-schedule operation). The

A_8 was controlled by means of two manual potentiometers: one for setting a nominal area and one to allow up to a full-scale deviation from this nominal area.

Both the CIVV and the A_8 control systems provided an option for selecting control by a digital computer, which will be used in future testing. Also, both control systems were provided with a digital voltmeter for smoothing adjustments preparatory to transfer of control. Comments regarding use of these control systems can be found in reference 1.

Fuel Control Modification

The engine has a hydromechanical (unified) fuel control, which provides basic scheduling of the engine, and an engine electronic control, which provides fine trimming commands to the engine. The control system manages engine operation by manipulating the CIVV, the rear compressor variable vanes (RCVV), the gas generator fuel flow, the augmentor fuel flow, and the exhaust nozzle. (The RCVV are the core-compressor-inlet vanes and the first two rows of core compressor stators, all of which are variable.)

It was decided that it would be better to assume direct control of the CIVV and the exhaust nozzle (as described previously) than to feed erroneous information to the engine fuel control to induce off-schedule operations. As a result, the control linkages from the engine fuel control to the CIVV and A_8 actuators were disconnected. It was believed (and, subsequently, verified experimentally) that these modifications would allow enough control to provide the necessary off-schedule operations of the engine without any adverse effects from the engine unified control.

The overall result was that the engine unified control monitored engine operation and maintained the core engine on the appropriate schedule while allowing off-schedule operation of the fan module. It should be noted that in this particular engine design the core compressor operating point appears to be comparatively insensitive to exhaust nozzle excursions. Further, it should be mentioned that normal engine unified control schedules in the operational regions of concern for stall flutter investigations call for the engine electronic control to be inoperative.

ENGINE INSTRUMENTATION

Aerodynamic Instrumentation

A wide variety of aerodynamic instrumentation was incorporated in the engine for this test series. The location and arrangement of this instrumentation are detailed in figure 6. Reference 1 contains an in-depth review of the nature and use of this instrumentation, and, thus, remarks made herein are general.

All thermocouples used were of the Chromel-Alumel junction type, measuring total temperature. Some thermocouples incorporated a shield, which brought the air around the thermocouple to stagnation; the rest were unshielded and had a Mach number correction applied to their output.

The pressure sensing instrumentation is straightforward and only a few remarks concerning the high-response pressure transducers (HRPT) will be made. The HRPT's are temperature sensitive and to minimize the effect, water-cooling jackets were incorporated on some of them. Although an effort was made to make all instrumentation rakes as thin as possible, the water-cooling jacket did represent a lower bound on HRPT rake width (0.64 cm (0.25 in.)). Wherever possible, the HRPT rakes and static tap adapters were designed to maintain a flat amplitude response to within ±5 percent up to an operational frequency of 500 hertz.

It should be noted that within the fan module the rakes were vane rakes and that at stations 2.0 (fan inlet) and 2.5 (core compressor inlet and fan bypass duct inlet) they were probe-mounted rakes. Vane rakes within the fan module were selected to avoid the unacceptably high blockages between stator blades that would have occurred with conventional rakes.

Structural Dynamic Instrumentation

Extensive dynamic strain-gage coverage consisting of 90 rotating and 24 stationary strain gages was used in the three fan stages of the engine to detect and analyze flutter. The locations of these gages are given in figure 7, and the operating stress limits for each type of gage are given in table I. The gages were placed on the blades in such a manner that each gage responded predominantly to one mode of blade vibration, thus simplifying the problem of identifying vibratory modes and applying safety stress limits during test operations. The gage locations were determined by the engine manufacturer by bench testing the blades involved. This testing involved holographic analysis of blade-alone vibrations for the blades of all three fan rotors and of blade-disk vibrations for the first fan rotor.

The strain gages and lead wires were installed by the engine manufacturer. The strain gage application procedure is as follows. (Exact adherence to this procedure could not be verified. A cross section at an exaggerated scale of a typical application appears in fig. 8.) The parts to which strain gages were to be attached were cleaned of all grease, oil, and metal chips. The work area and tools were in a similarly clean condition. The areas not to be sandblasted were double-masked off with 3M No. 470 Yellow masking tape PMC 4134. The parts were sandblasted using No. 30-grit aluminum oxide.

The masking tape was then removed, and the parts washed with running water, allowed to dry, and washed again with clean acetone applied with clean tissues. The cleaned surfaces were to be given special handling to avoid their being touched by human skin (which might have left a grease print). After cleaning, the areas to be instrumented were masked again with 3M No. 545 pressure-sensitive tape to control overspray during flame spraying. Aluminum foil was also used to mask large areas. The areas to be instrumented were then flame sprayed with a 0.092- to 0.152-millimeter (0.004- to 0.006-in.) thick coat of Rokide-A rod (Al_2O_3) of 98.6 percent purity. This completed the surface preparation.

To install the gages, the following steps were taken: The strain gages were set in position with the paper carrier up and temporarily secured with masking tape. Rubber strips were placed between the gage grid and the tape. A thin coat of ceramic cement was applied to the gage loops and allowed to dry for 30 minutes. This was followed by high-temperature drying (using a hair dryer placed approx. 20 cm (11 in.) from the strain gages) for 10 minutes. The tape was then removed, and the paper carriers soaked in acetone and carefully removed. The parts were then washed with acetone to remove all paper carrier and tape residues. The cement was cured in an oven for 30 minutes at 338 K (150° F) followed by a slow ramp to 616 K (650° F). The second temperature was held for 1 hour. The oven was then turned off, and the part allowed to cool to below 338 K (150° F) before it was removed from the oven. At this point, the part was inspected to determine whether the grid wires were taut, whether the gage resistance was appropriate, and whether leakage to ground was greater than 20 megohms. Following this, the gage cementing was completed with a thin coat of ceramic cement over the uncemented portions of the gage followed by the curing cycle previously described. The nickel ribbon leads were secured by flame spraying the part with Rokide-A rod. The leads were held in place for flame spraying by 0.63-centimeter (0.25-in.) wide pieces of 3M No. 545 tape placed at 0.63-centimeter (0.25-in.) intervals. After an initial flame spray of the ribbons, the tape was removed, and the exposed areas were flame sprayed. The thickness of the flame-spray material was not allowed to accumulate nor was it allowed to cover the ceramic cement. Any excess material was removed by sanding with aluminum oxide rod. The entire area was finally given a 0.008- to 0.013-centimeter (0.003- to 0.005-in.) thick coat of ceramic cement (using a spray gun or a camel's hair brush for hard to reach areas) followed by a coat of very high-temperature paint to resist moisture and resulting leakage to ground.

The nickel-ribbon lead wires applied with the strain gages were routed along the blade toward the root and over the blade-to-disk jump where they were spliced to round, high-temperature, insulated lead wires. These round lead wires were routed through the interior of the fan disk assembly to a 100-pin connector at the front of the assembly on the engine axial centerline. (General lead-wire routings are shown in fig. 9.) Wires then led from the mating half of the 100-pin connector to the engine side of a 100-channel, Freon-cooled, high-speed slip ring (fig. 10). Figure 11 shows more detail of the strain-gage - lead-wire clamp assembly, which was devised especially for this use.

Originally, a common, floating ground system was used to pass the signals from all 90 rotating strain gages through the 100-channel slip ring. But during engine operation the floating ground accidentally grounded itself to the engine (a significant source of electrical noise), which caused all 90 strain gages to be overpowered with electrical noise. As a result, 48 of the strain gages were rewired with two slip-ring channels per strain gage (individual floating ground system).

Strain-gage mortality was of concern to both current and future testing; therefore, records of strain-gage failures were kept. Tables II and III, for rotating strain gages only, are examples of the kinds of records kept. Figure 12 is a semilog plot of strain-gage mortality as a function of run time. From this figure one can deduce an approximate half-life for the strain gages of about 16 hours; however, the wide data scatter throws considerable suspicion on both the value of the calculated number and on the validity of the exponential decay model in describing the failures. Thus, it should be recognized that the half-life value is offered solely as a rough guide in the absence of a more comprehensive performance index.

Upon the completion of testing, the fan module was removed and disassembled for replacement of strain gages and for the incorporation of additional instrumentation. In the course of this disassembly, the strain-gage system was carefully inspected to identify the strain-gage failure modes. The information was used to formulate modifications to the installation procedure in order to obtain longer usable strain-gage life.

As is shown in figure 13(a), the predominant identifiable failure was caused by the erosion of the aluminum oxide flame-spray outer coating on the lead wires and the attendant debonding of the lead wires, followed by a disruption of the nickel-ribbon lead-wire circuit. Of main concern is the source of the erosion and/or debonding of the flame spray.

The theory first advanced was that the inlet air contained such a supply of dust, grit, and other foreign objects, such as rust scale, that the effect was like a continuous sandblasting of the coating which, consequently, removed the flame-spray coating and destroyed the strain-gage and/or lead-wire continuity. This theory cites as substantiation the photographically recorded fact that the erosion occurred primarily on the concave side of the blade (fig. 13(a)), where particles would naturally impact the surface, while the coatings on the convex side of the blade (fig. 13(b)) were relatively undamaged. Although it is known that the facility air-supply system contains rust and grit, no data are presently available concerning the size and quantity of the impurities.

A more careful study of figure 13 reveals the high level of erosion immediately over the lead wires and the lack of increasing spanwise severity toward the tip (due to higher relative ''sandblasting'' velocities). This suggests that the erosion was intensified by lumps in the coating caused by the presence of the lead wires.

With regard to a possible bond shortcoming, several points should be noted. First, there would appear to be an absence of bond between the underside of the ribbon lead wire to the flame-spray base coat. This in itself could be significant in that the flame spray over the lead wires was bonded only to the spaces between the lead wires. Second, one may reasonably expect some incompatibility in rigidity between the titanium blade, the aluminum oxide coating, and the nickel ribbon, which would lead to very high stresses in the nickel wire and possibly the aluminum oxide coating due to flexure and distance from the neutral axis. Also, such incompatibilities could lead to high interlaminar shear stress, which, in turn, could lead to debonding. Third, these difficulties would be aggravated by excessively thick aluminum oxide layers.

These points indicate that even with impurities in the inlet air, the life of the strain-gage installation can be increased by improving the bond quality (including bonding all sides of lead wires), by keeping flame-spray coatings thin and properly contoured and by seeking methods of relieving material rigidity incompatibilities.

DATA ACQUISITION SYSTEMS

Recording Systems

Normal data recording was accomplished by three systems: the central automatic digital data encoder (CADDE), the transient data recorder (TRADAR), and the central analog recording system (CARS). The CADDE system was composed of two subsystems: the digital automatic multiple pressure recorder (DAMPR) and the automatic voltage digitizer (AVD). The CADDE system was designed to gather steady-state data, transient data were gathered in digitized form by the TRADAR and in analog forms by the CARS. The TRADAR system is capable of digitizing at an overall rate of 30 kilohertz; however, a rate of approximately 4. 8 kilohertz overall was used throughout these tests.

The DAMPR part of the CADDE systems recorded the values of up to 450 steady-state pressures by measuring the time span between the opening of an air-supply valve to an evacuated tank and the equilibration of each pressure measurement line. Calibration is achieved by a calibration chart for each orifice and tank combination and by the measurement of both a high and a low reference pressure. From this information the values of the data pressures are determined and stored on the CADDE magnetic tape systems.

The second subsystem of the CADDE is the AVD. The system scans the voltage output of a wide variety of steady-state transducers (other than pressures covered by the DAMPR), digitizes the voltages locally, and transmits the output to the central recording facility of CADDE. Voltages digitized by AVD originate from instrumentation such as thermocouples, pressure transducers, and speed indicators. Selection of input data to the digitizer was done by means of solid-state switching circuitry.

The CADDE had, during this test series, the capacity to store 500 words of DAMPR and 500 words of AVD information, although the facility did not need to utilize this full capability. A diagram of CADDE components is included in figure 14.

The second data recording facility used was the TRADAR. The system achieved much the same results as AVD, but with several differences in equipment and a large increase in speed. The system consisted, basically, of a central recorder, a central subsystem, and a series of facility subsystems. Each subsystem had a capacity of 200 channels, each with a digitizing amplifier. During this test, PSL used all 200 channels of TRADAR. Facility subsystems necessarily had the gains of these amplifiers set manually. Each subsystem transmitted its data sequentially through a single cable to the central recorder. In scanning channels for recording, control was given to a 1000-word programmable central core memory, which contained a sequence of words indicating the address and gain setting of each channel that was to be sampled and recorded. When sample rates were below 16 000 per second, no restrictions were placed on sampling order by the system. The maximum overall sampling rate was 30 000 per second. An additional feature of the facility subsystems was that the first 50 amplifiers have auxiliary outputs, which were usually used for driving control room or facility displays. Data were ultimately recorded on digital magnetic tape. Figure 15 is a schematic diagram of the TRADAR system.

The third and last major data acquisition system was the CARS. This was the main means for recording high-response transient data, most notable among these being the dynamic strain-gage signals that were recorded solely on this system. Other high-speed data, such as those from certain high-response pressure transducers along with engine parameter data, were also recorded on this system for the purpose of correlating these with strain-gage data.

Data were transmitted from the test facility to the CARS via two 100-pair shielded cables. These cables were designed to have acceptable response characteristics up to 10 kilohertz. These signals were then directed to 180 voltage-controlled oscillators with frequency response capabilities to 4 kilohertz. (Other voltage-controlled oscillators were used for recording system reference signals.) These signals were then multiplexed to provide a recording on magnetic tape of 15 channels on each of 12 tracks for a system capability of 180 lines of continuous analog data. Calibration signals of zero, half scale, and full scale were always recorded at the beginning of each analog tape by the CARS facility; similar zero, half-scale, and full-scale calibration signals for strain-gage signals only were recorded at the beginning of each CARS recording point by the test facility.

To obtain sufficiently high frequency response, tape speeds were quite high (305 cm/sec (120 in./sec)). Because of the attendant tape consumption problem, the analog data were taken only when they appeared valuable. Figure 16 is a diagram of the CARS.

Two additional data recorders should be mentioned: The first was an on-site 42-channel FM analog recorder. This recorder was able to rerun data either immediately or on a morning-after basis for two purposes: to direct further testing or to identify data requiring further processing in the central facility. The other recording system consisted of two 14-channel FM tape recorders having a variety of engine health and safety signals as inputs. These records are only of interest if an engine or facility-related anomaly occurs. These tape recorders were left on for all engine operations.

Data Monitoring Systems

The identification of flutter and its onset were tasks of great importance in this test series. Indeed, probably the most serious aspect of the flutter phenomenon is that it can go totally unnoticed by general aerodynamic instrumentation until it results in catastrophic engine failure. In this test series, flutter was identified through the monitoring of dynamic signals from strain gages located in strategic positions on the appropriate blades as noted previously.

Direct monitoring of all strain-gage signals was accomplished by observing the raw signals on 5.08-centimeter (2.0-in.) wide oscilloscopes, which were triggered by a low-pressure-rotor once-per-revolution speed signal. To more positively identify vibratory mode shapes and to screen out noise, two frequency spectrum analyzers (with interconnected large oscilloscopes) were also used for the on-line analysis of any two strain-gage signals (fig. 17).

A further aid in strain-gage signal monitoring was a signal microprocessor which provided not only signal conditioning and amplification but also continuous, sequential scanning of signals for amplitudes in excess of the preset limits (table I). The microprocessor sounded alert and abort alarms, as appropriate, and displayed the channel number of the first offending gage. Details of the microprocessor system are contained in reference 3.

Because this type of testing is comparatively new and experience with the monitoring signals from such testing is not widespread, it is important to make a few comments about the operations of monitoring procedures. At the outset of testing 114 stationary and rotating strain gages were to be monitored. Five engineers were assigned to monitor the signals and to direct the testing based on these signals. Two engineers monitored (and analyzed) the first rotor gages (which were thought to be the most important), two more the second and third rotor gages, and the fifth the stator gages. Although this proved acceptable in terms of the ability to scan the small oscilloscopes quickly enough to pick and validate signals in a timely manner, it also proved to be congested in front of the oscilloscopes. Further, this approach occasionally led to a lack of coordination among the engineers.

Another consideration in the monitoring process was the time to obtain a frequency spectrum analysis. As noted before, the spectrum is highly useful for identifying flutter modes, engine-induced blade vibrations, and general noise. Since the spectral analyzers used were essentially sweeping band-pass filters, accuracy required time. In many cases a fast inaccurate spectrum is as useless as a slow accurate spectrum is dangerous. Thus, the observer must seek a balance between speed and accuracy. In future flutter testing a fast Fourier transform element attached to the microprocessor, as well as a digital fast Fourier transformer, will provide additional spectral analysis.

An additional aid to later analysis, as well as to immediate orientation of the data, was a manual time marker which marked the occurrence of flutter. It placed an electrical marker on a channel of the CARS tape and stopped the local clock display so that the observers could note the time of the onset of flutter.

Even with all these data monitoring facilities, distinguishing flutter and nonflutter modes of vibration was still difficult. There is currently no way to observe the physics of the aerodynamic-structural elastic coupling, which is the trademark of flutter. High vibratory levels alone are not conclusive. The frequency of vibration of flutter is thought to be independent of engine speed; however, this is not to say that this frequency cannot, by chance, occur at an even multiple of engine rotational frequency. Rapid, conclusive, on-line identification of flutter is not easy to achieve. Perhaps the best approach for confirming flutter on-line is to vary the operating speed of the engine and watch for any changes in the frequency of the strain-gage signals. The true flutter may or may not be independent of speed; however, any dependence on speed should not be similar to other known forms of blade vibration which are speed dependent (e.g., vane wake passing frequencies).

CONCLUSION

This report has detailed the installation and instrumentation of a turbofan engine for an experimental investigation of fan aeroelastic instabilities. A number of problem areas arose during the course of the testing; however, most could be cured during the course of testing or during hardware modifications for subsequent test series. Problems associated with obtaining off-schedule engine operations, automatic data monitoring, and flutter identification are reasonably under control.

One area which promises to be a continuing problem is the durability of the dynamic strain-gage installations. The installation in this engine was only marginally adequate for aeroelastic testing purposes because of its fragility in comparison with the required length and severity of testing. A more reliable procedure should be found to instrument blading for structural vibrations.

Lewis Research Center,
National Aeronautics and Space Administration,
Cleveland, Ohio, March 23, 1977,
505-05.

REFERENCES

1. Mehalic, Charles M.; Hurrell, Herbert G.; Dicus, John H.; Lubomski, Joseph F.; Kurkov, Anatole P.; and Evans, David G.: Experimental Results and Data Format of Preliminary Fan Flutter Investigation Using YF100 Engine. NASA TM SX-3444, 1977.
2. Central Automatic Data Processing System. NACA TN 4212, 1958.
3 Smalley, Robert R.: Microprocessor-Based Multichannel Flutter Monitor Using Dynamic Strain Gage Signals. NASA TM X-71884, 1976.

TABLE I. - IMPOSED VIBRATORY STRESS LIMITS

Strain-gage number	Strain-gage location[a]	Warning limit		Never-exceed limit	
		MPa	ksi	MPA	ksi
101-106	1st rotor, tip	69	10	138	20
107-114	1st rotor, ASMT	34	5	69	10
115-120	1st rotor, ASTE	34	5	↓	↓
121-128	1st rotor, SHRD-CX & CC	28	4	↓	↓
129-132	1st rotor, RMT	↓	↓	↓	↓
133-136	1st rotor, FILLET	↓	↓	34	5
137-140	1st rotor, D-WEB	↓	↓	34	5
201-205	2nd rotor, tip	55	8	138	20
206-210	2nd rotor, ASMT	34	5	69	10
211-213	2nd rotor, ASTE	34	5	↓	↓
214-220	2nd rotor, SHRD-CX & CC	28	4	↓	↓
221-224	2nd rotor, RMT	28	4	↓	↓
225-228	2nd rotor, D-WEB	28	4	34	5
301-305	3rd rotor, tip	34	5	138	20
306-309	3rd rotor, ASMT	34	5	69	10
310-315	3rd rotor, SHRD-CX & CC	28	4	↓	↓
316-318	3rd rotor, RMT	28	4	↓	↓
1-4	1st stator, ODLE	34	5	↓	↓
5-8	1st stator, ODMT	↓	↓	↓	↓
9-12	1st stator, MSMT	↓	↓	↓	↓
13-16	2nd stator, ODMT	↓	↓	↓	↓
17-20	2nd stator, ODTE-CX & CC	↓	↓	↓	↓
21-24	2nd stator, MSMT	--	--	--	--

[a]See fig. 7.

TABLE II. - ACTIVE ROTOR STRAIN GAGES

Rotor number	Number of strain gages installed	Date					
		2/19/75	4/4/75	4/10/75	4/25/75	5/1/75	6/1/75
		Number of strain gages working					
1	40	38	33	28	27	27	12
2	28	28	24	19	18	18	6
3	22	22	18	12	9	6	6
Total	90	88	75	59	54	51	23
	Accumulated run time, hr:min						
	0	18:33	21:17	24:36	31:02	38:32	42:30
	Accumulated engine starts						
	0	9	10	12	14	15	17

TABLE III. - STRAIN-GAGE FAILURE SUMMARY

(a) Rotor 1

Strain-gage number	Date of failure	Remarks
101	4/4/75	Intermittent ground
106		
111		
112		
118		
105		Open circuit (as supplied)
138		
115	4/8/75	Open circuit, interacted with signals to data center causing extreme noise
125		Intermittent ground
126	4/8/75	
127		
128		
110	4/18/75	Open circuit

(b) Rotor 2

Strain-gage number	Date of failure	Remarks
204	4/4/75	Intermittent ground. Caused very noisy signals throughout entire strain-gage system
202	3/27/75	Failed, cause unknown
212		
227		
207	4/8/75	Intermittent ground
215		
218		
219		
220		
226	4/18/75	Open circuit

(c) Rotor 3

Strain-gage number	Date of failure	Remarks
311	3/27/75	Failed, cause unknown
317		
319		
321		
303	4/8/75	Failed, cause unknown
304		
310		
312		
313		
314		
315	4/18/75	Open circuit
316		
318		

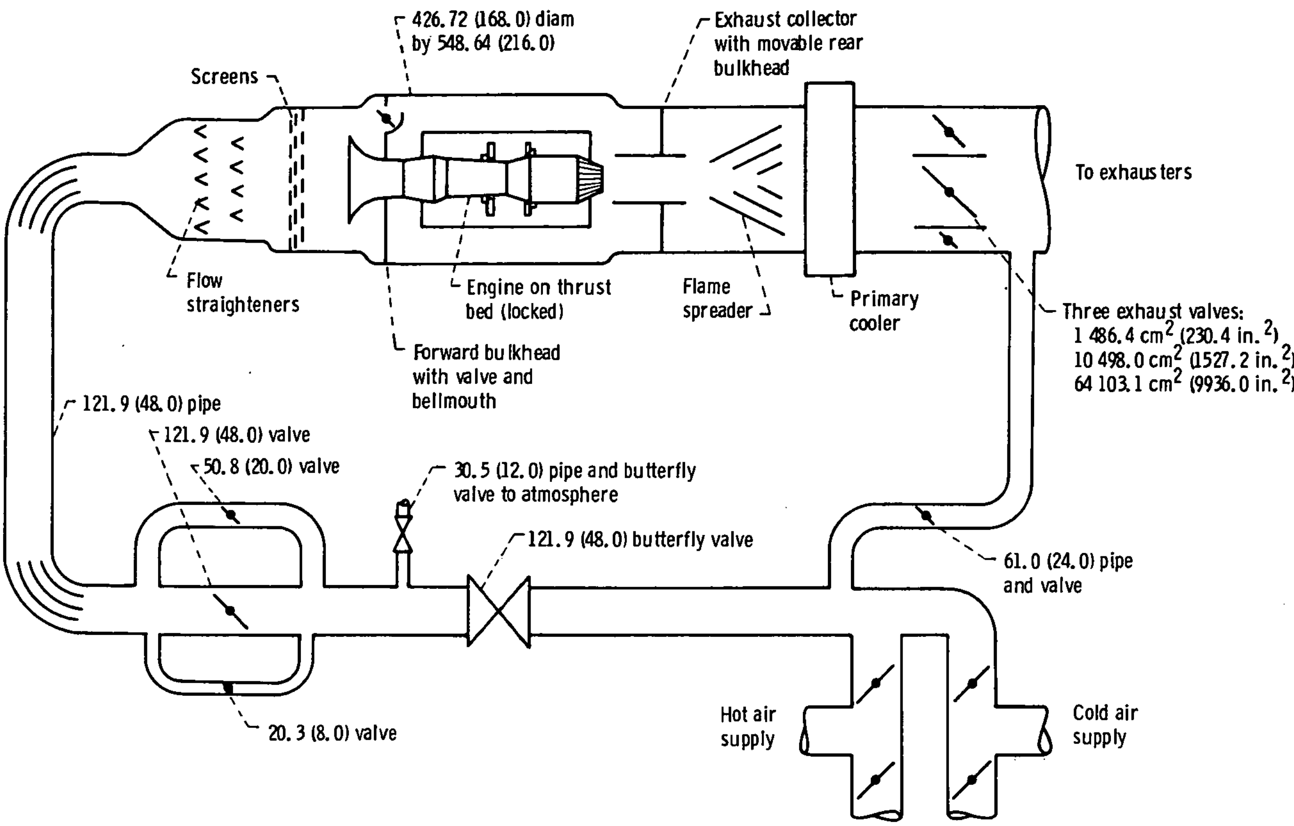

Figure 1. - Schematic diagram of the propulsion systems laboratory cell 1. (Note: Drawing not to scale. Dimensions are nominal in cm (in.) except as noted.)

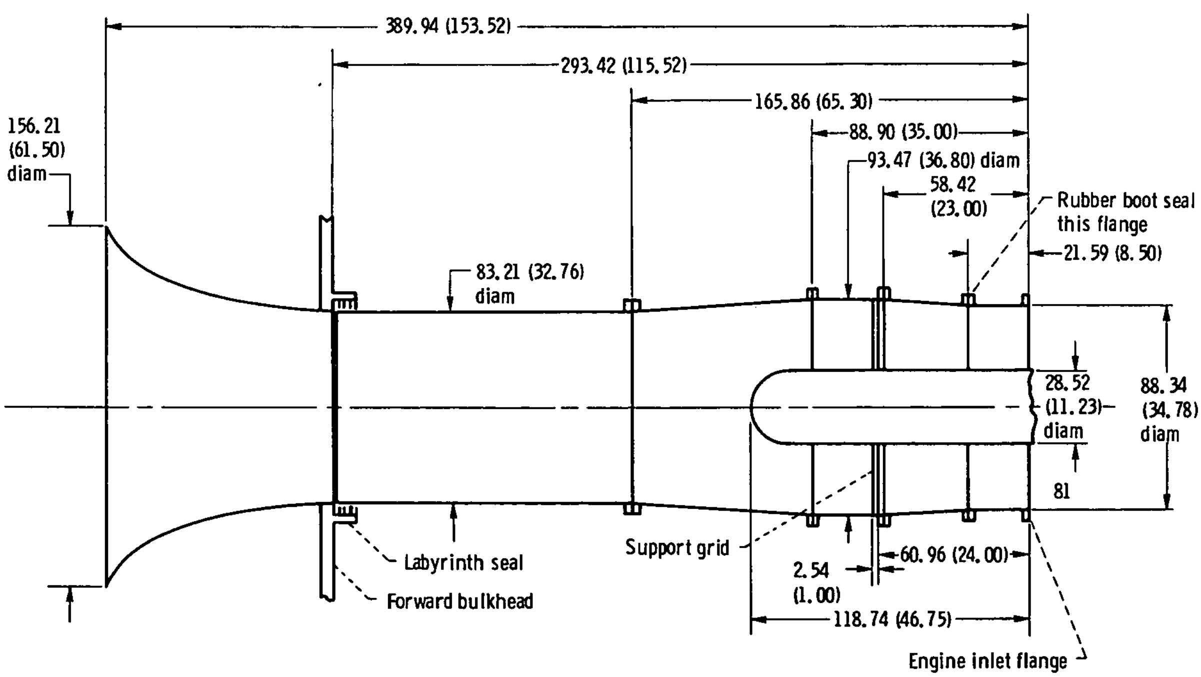

Figure 2. - Engine inlet detail. (Drawing not to scale. Dimensions are nominal in cm (in.).)

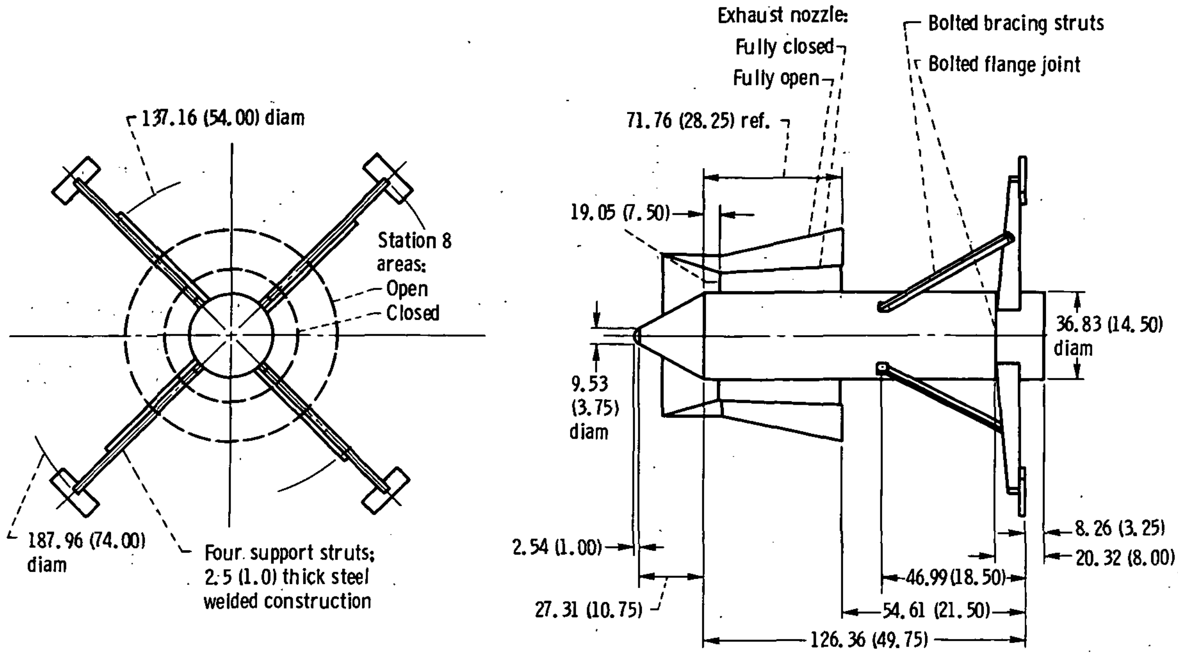

Figure 3. - Exhaust nozzle plug - stretched. (Notes: Dimensions are nominal in cm (in.). Drawing not to scale.)

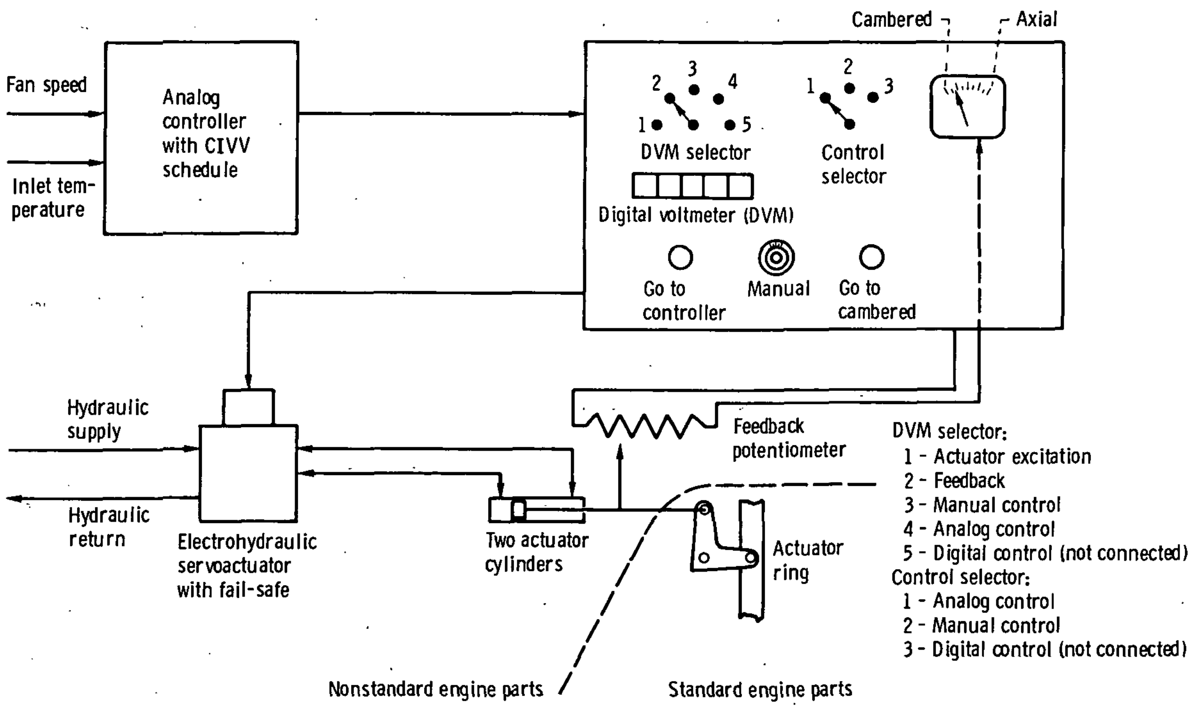

Figure 4. - Compressor-inlet variable vanes (CIVV) command-actuation system. All nonstandard parts except actuator ring and two links.

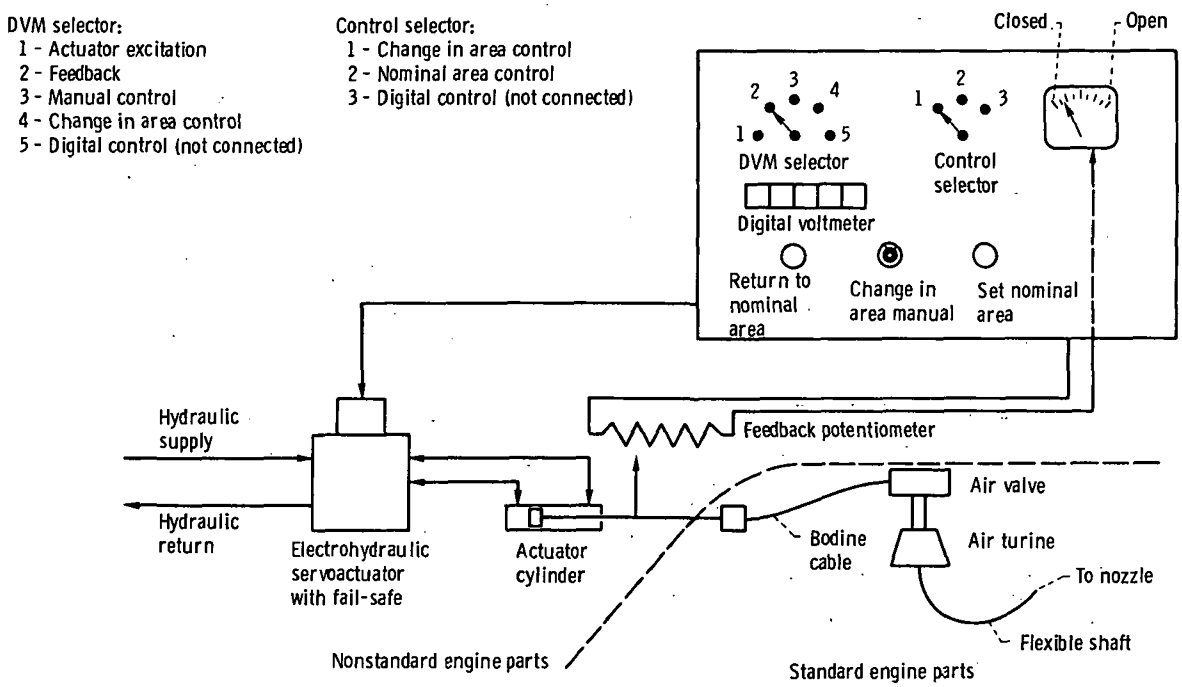

Figure 5. - Exhaust nozzle (A_8) command-actuation system.

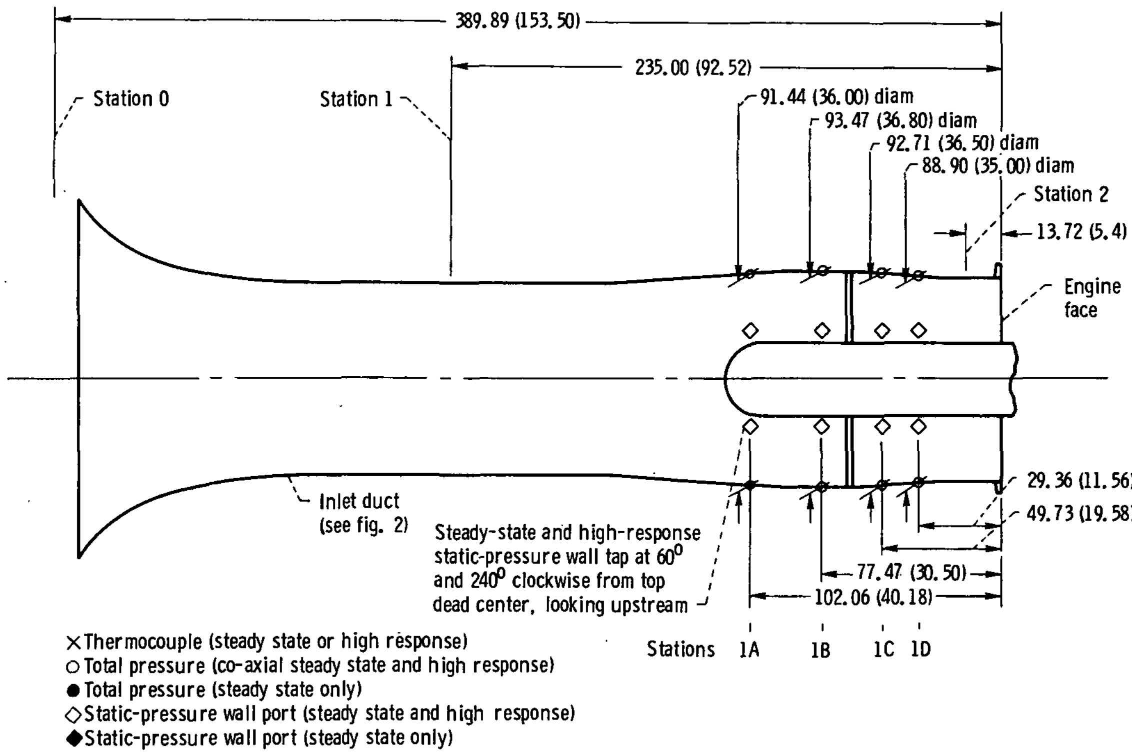

(a) Inlet duct instrumentation stations.

Figure 6. - Engine and inlet duct aerodynamic instrumentation. (Notes: Drawing not to scale. Dimension are nominal in cm (in.) unless otherwise stated.)

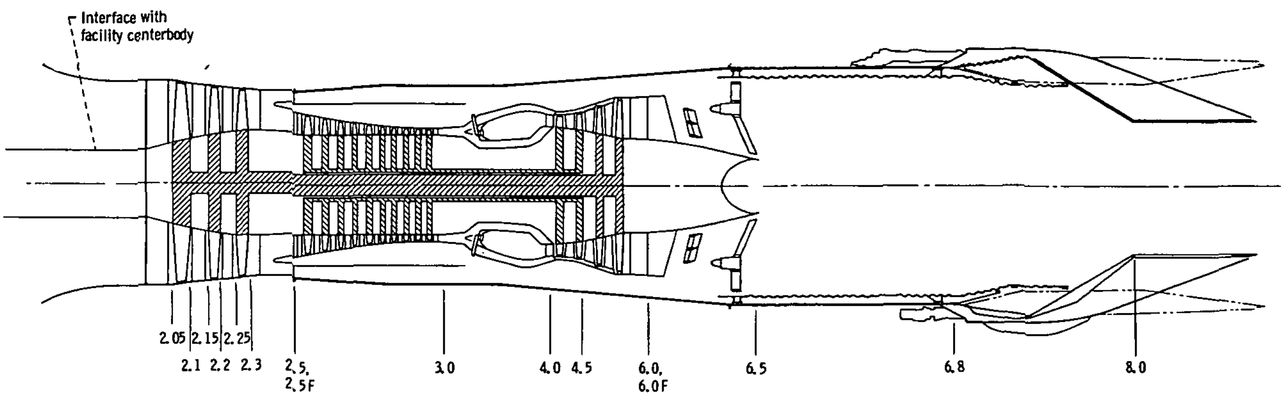

(b) Engine instrumentation stations.

Figure 6. - Continued.

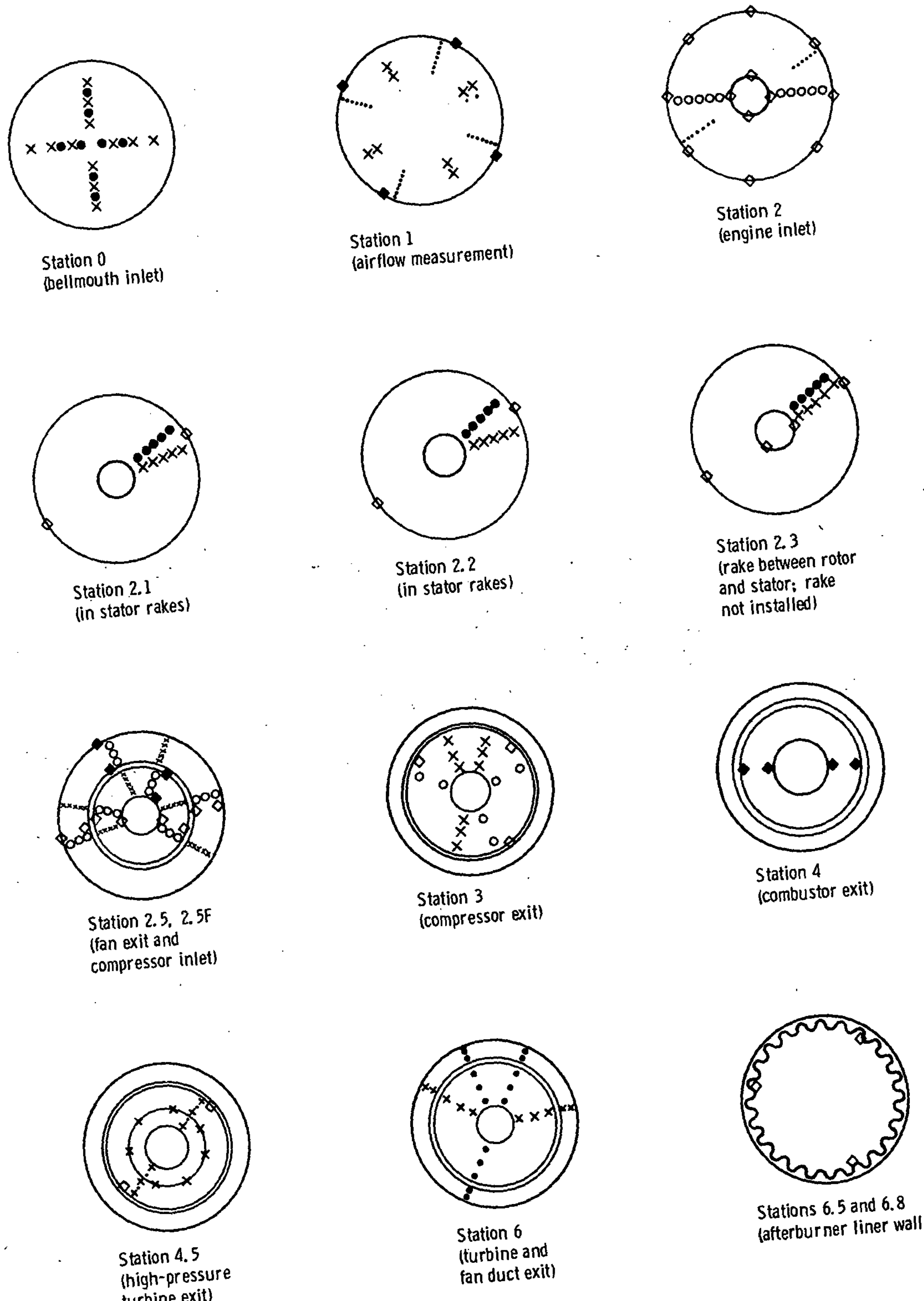

(c) Inlet duct and engine measuring stations (looking upstream).

Figure 6. - Concluded.

	Strain-gage grid size	Strain-gage location
	0.7938 (0.3125) by 0.2381 (0.0938)	Airfoil, concave surface
	0.7938 (0.3125) by 0.2381 (0.0938)	Airfoil, convex surface
	0.7938 (0.3125) by 0.2381 (0.0938)	Web, disk
	0.3178 (0.1250) by 0.1588 (0.0625)	Shroud or fillet (fillet rotor 1 only)

ASMT	Above shroud, maximum thickness
ASTE	Above shroud, trailing edge
SHRD CX	Shroud, convex side
SHRD CC	Shroud, concave side
RMT	Root, maximum thickness
D-web	Web, disk
ODLE	Outside diameter, leading edge
ODTE	Outside diameter, trailing edge
ODMT	Outside diameter, maximum thickness
MSMT	Midspan, maximum thickness

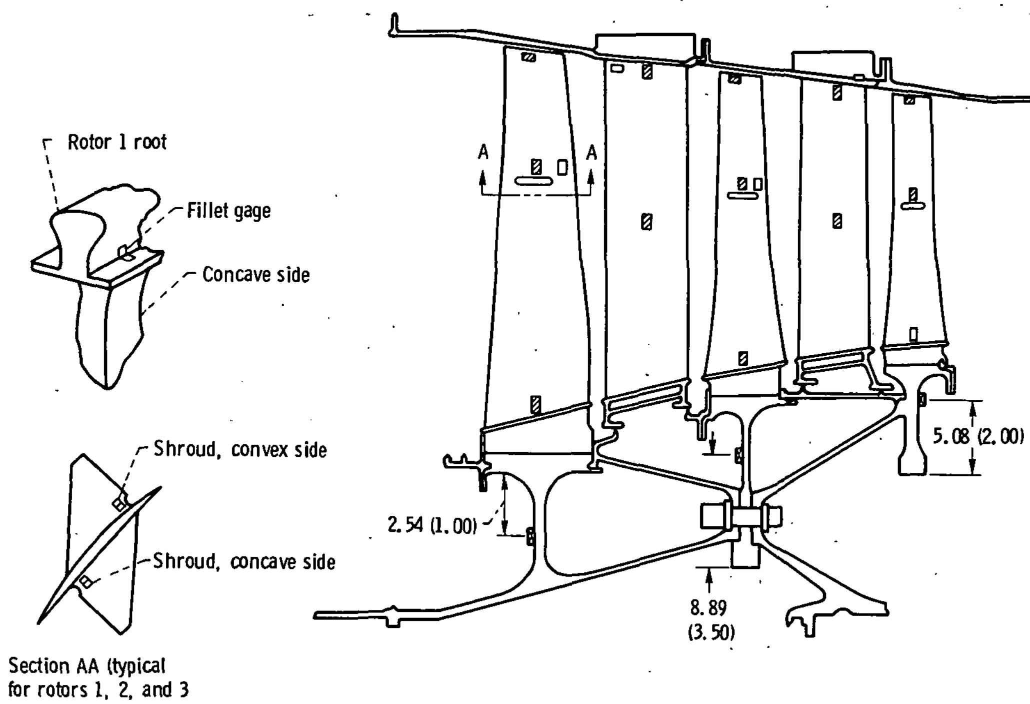

(a) Overall fan strain-gage locations.

Figure 7. - Structural dynamic instrumentation. (Dimensions are nominal values. Linear dimensions in cm (in.). Angles are clockwise from top dead center, looking upstream. Slot numbers are clockwise from top dead center looking upstream (slot 1 is top dead center). Drawings not to scale.)

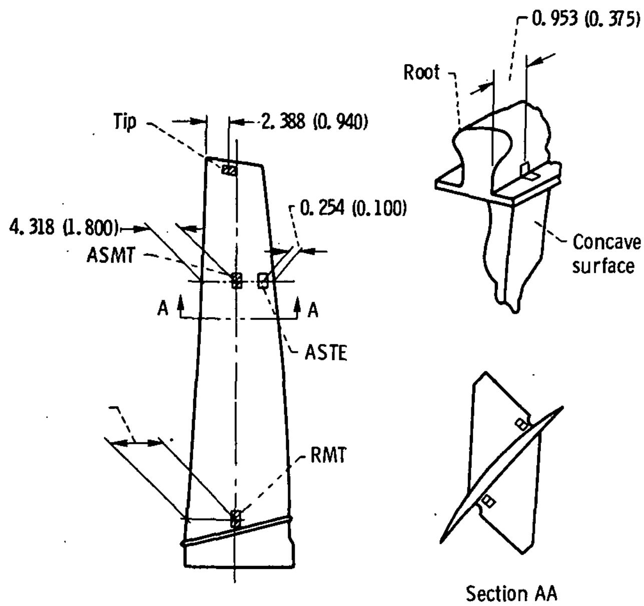

Strain-gage location	Angle, deg										Total
	0	17	95	142	170	180	190	227	275	313	
	Slot										
	1	6	11	16	9	20	21	25	30	34	
	Strain-gage number										
TIP	101	---	102	103	---	104	---	105	106	---	6
ASMT	107	108	---	109	110	111	112	---	113	114	8
ASTE	---	115	---	116	117	118	119	120	---	---	6
SHRD CX	121	---	122	---	---	---	---	123	---	124	4
SHRD CC	---	125	---	126	---	127	---	---	128	---	4
RMT	129	---	130	---	---	---	131	---	---	132	4
FILLET	---	133	---	---	134	---	---	135	---	136	4
D-WEB	137	---	138	---	---	139	---	140	---	---	4
											40

(b) First fan rotor blade. Total number of blades, 38.

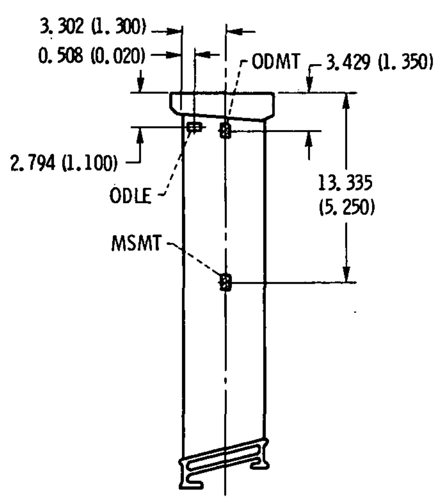

Strain-gage location	Angle, deg				Total
	0	90	180	270	
	Slot				
	1	14	27	40	
	Strain-gage number				
ODLE	1	2	3	4	4
ODMT	5	6	7	8	4
MSMT	9	10	11	12	4
					12

(c) First fan stator vane. Total number of blades, 52.

Figure 7. - Continued.

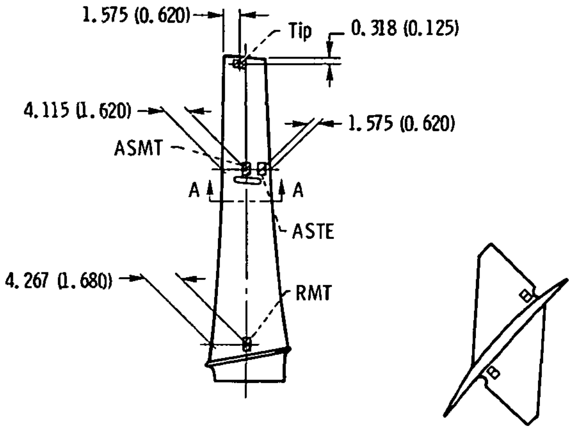

Section A-A

Strain-gage location	Angle, deg								Total
	0	48	90	138	180	228	270	318	
	Slot								
	1	9	16	24	31	39	46	54	
	Strain-gage number								
TIP	201	---	202	203	---	204	---	205	5
ASMT	206	---	207	---	208	209	---	210	5
ASTE	---	211	---	212	---	---	213	---	3
SHRD CX	214	---	215	---	216	---	217	---	4
SHRD CC	---	218	---	219	---	220	---	---	3
RMT	---	221	---	---	222	---	223	224	4
D-WEB	225	---	226	---	227	---	228	---	4
									28

(d) Second fan rotor blade. Total number of blades, 60.

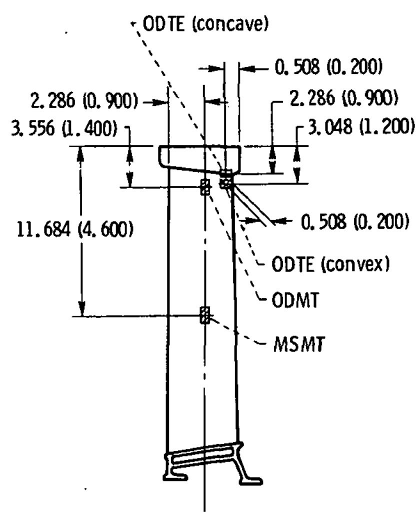

Strain-gage location	Angle, deg				Total
	0	90	180	270	
	Slot				
	1	15	29	43	
	Strain-gage number				
ODMT	13	14	15	16	4
ODTE CX	17	--	18	--	2
ODTE CC	--	19	--	20	2
MSMT	21	22	23	24	4
					12

(e) Second fan stator vane. Total number of fanes, 56.

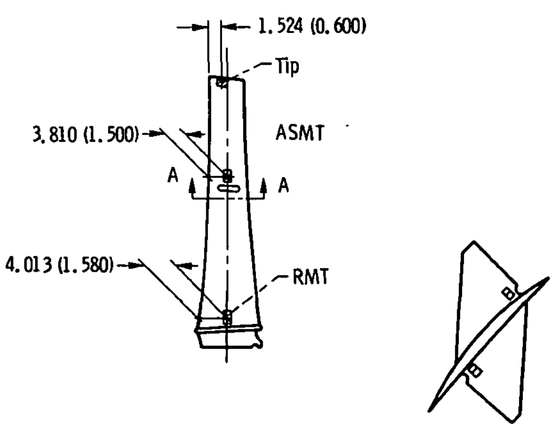

Strain-gage location	Angle, deg						Total
	0	60	120	180	240	300	
	Slot						
	1	7	14	22	30	37	
	Strain-gage number						
TIP	301	---	302	303	304	305	5
ASMT	306	307	---	308	309	---	4
SHRD CX	---	310	311	---	---	312	3
SHRD CC	313	---	---	314	315	---	3
RMT	---	316	317	---	---	318	3
D-WEB	319	---	320	---	321	322	4
							22

Section A-A

(f) Third fan rotor blade. Total number of blades, 46.

Figure 7. - Concluded.

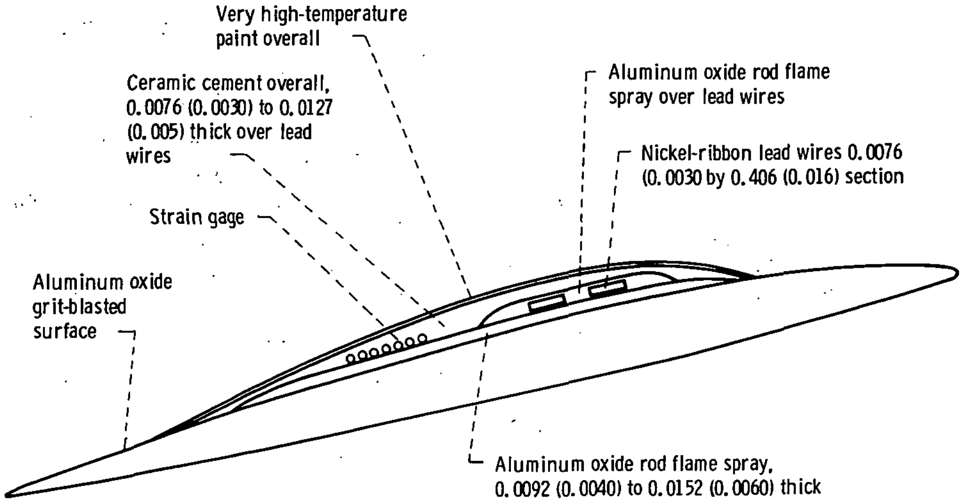

Figure 8. - Cross section of typical strain-gage and nickel-ribbon lead-wire application. (Drawing not to scale. Dimensions in cm (in.).)

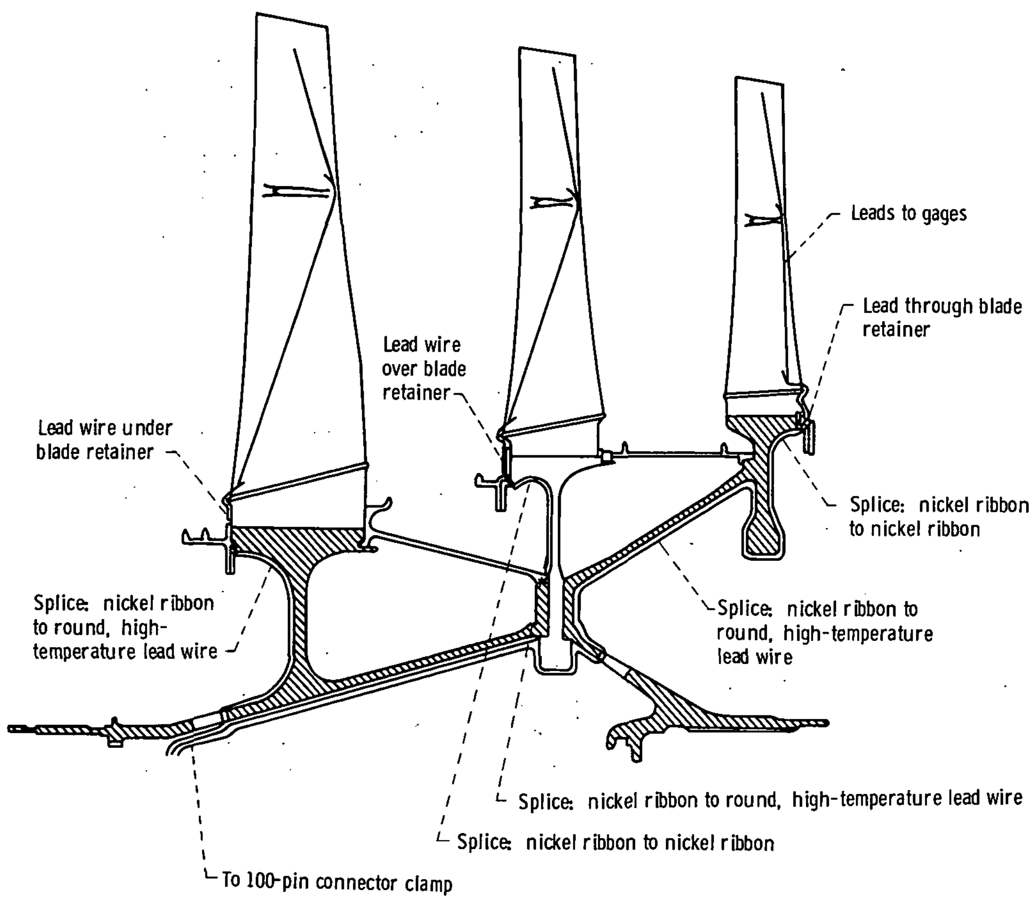

Figure 9. - Typical strain-gage lead-wire routings. (Notes: High-temperature lead wires were cemented in position throughout lengths. Drawing not to scale.)

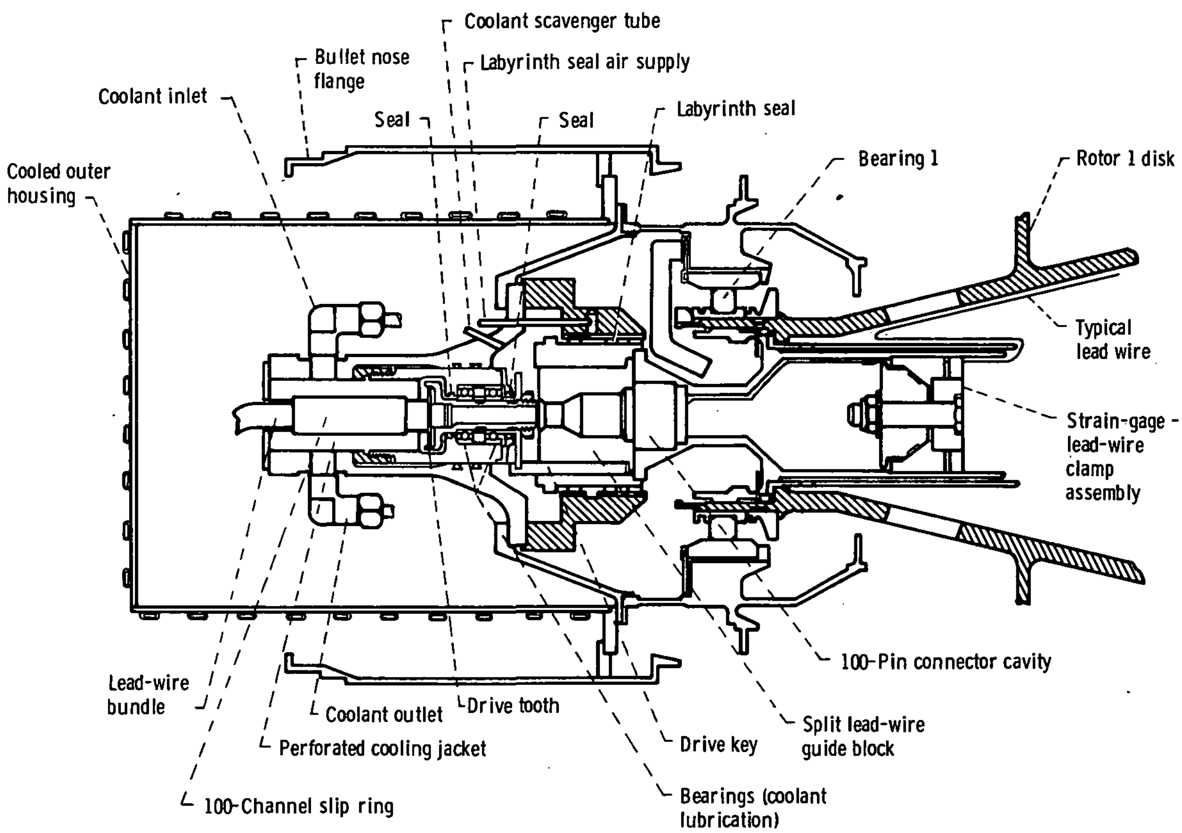

Figure 10. - Slip-ring installation. (Drawing not to scale.)

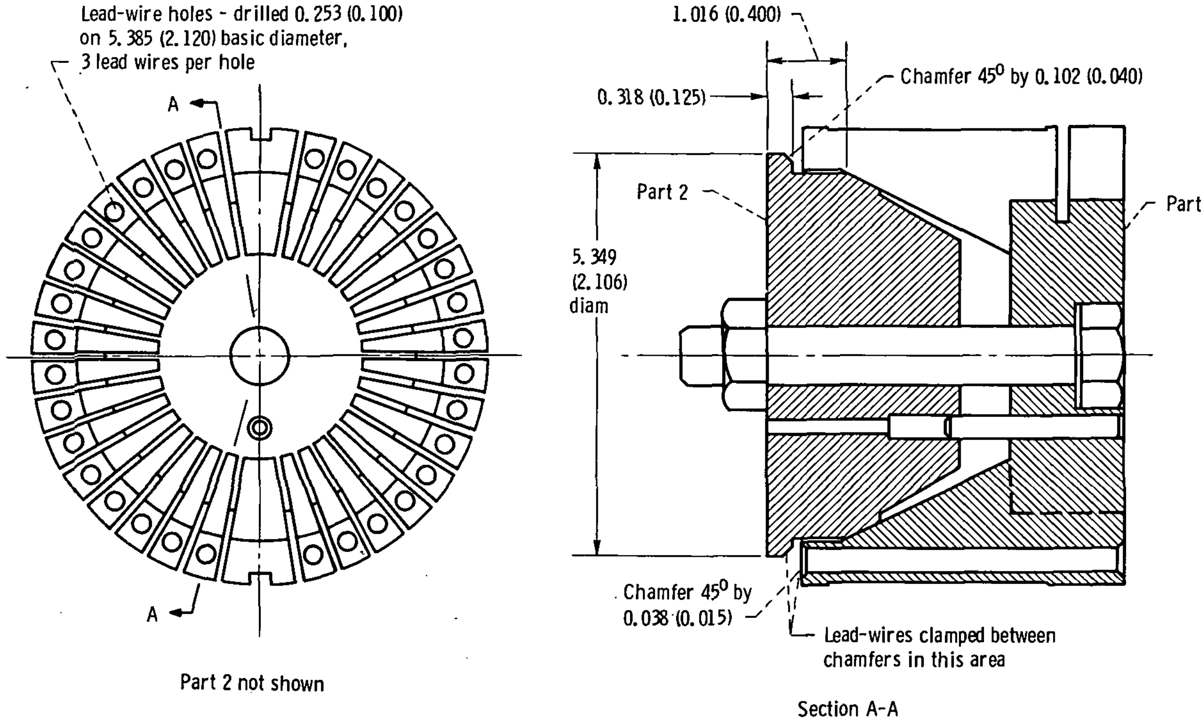

Figure 11. - Strain-gage and lead-wire clamp assembly. (Drawing not to scale.)

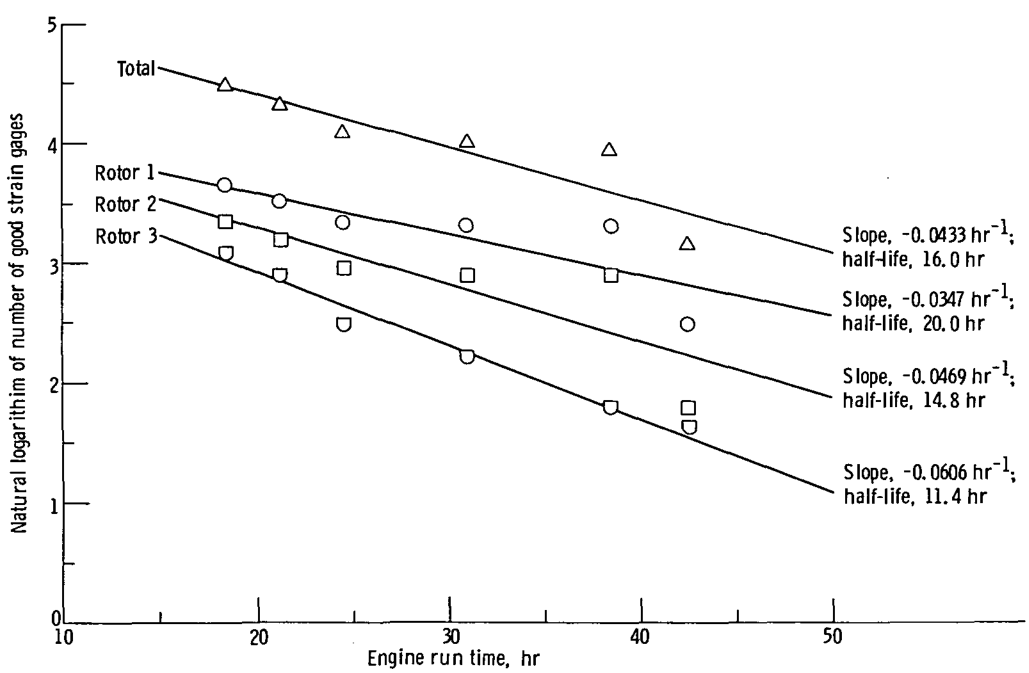

Figure 12. - Absolute mortality of strain gages against elapsed engine run time.

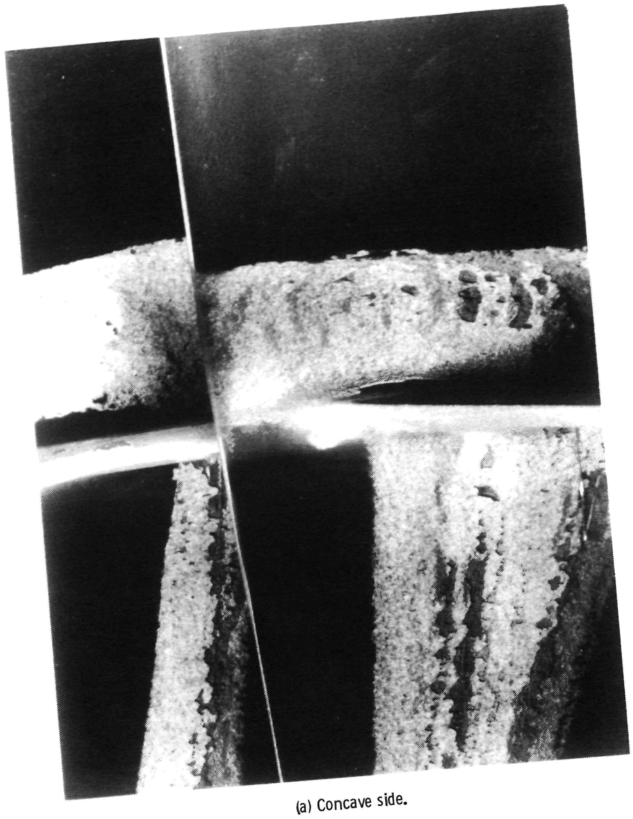

(a) Concave side.

(b) Convex side.

Figure 13. - Erosion of strain-gage and lead-wire coating on a first-rotor blade.

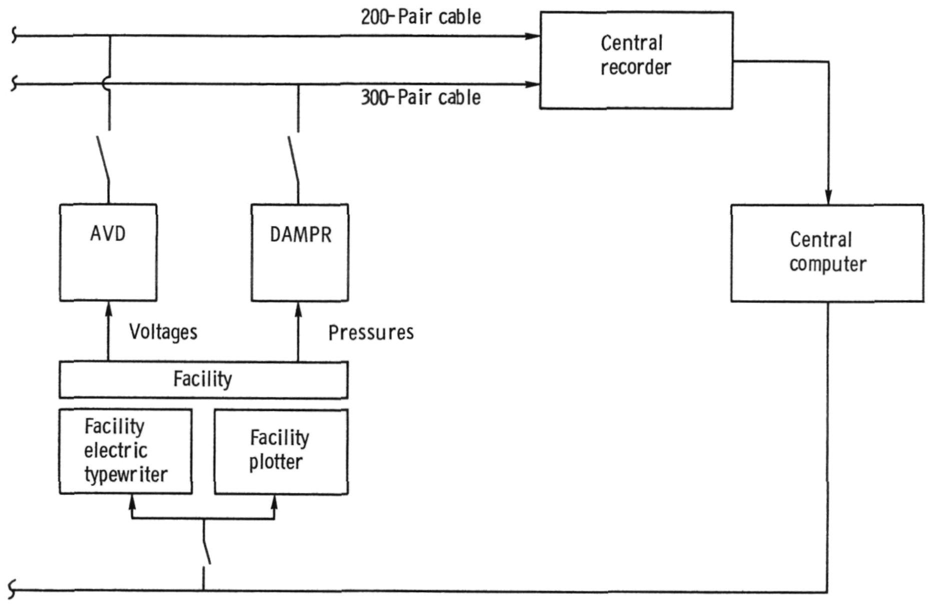

Figure 14. - CADDE system.

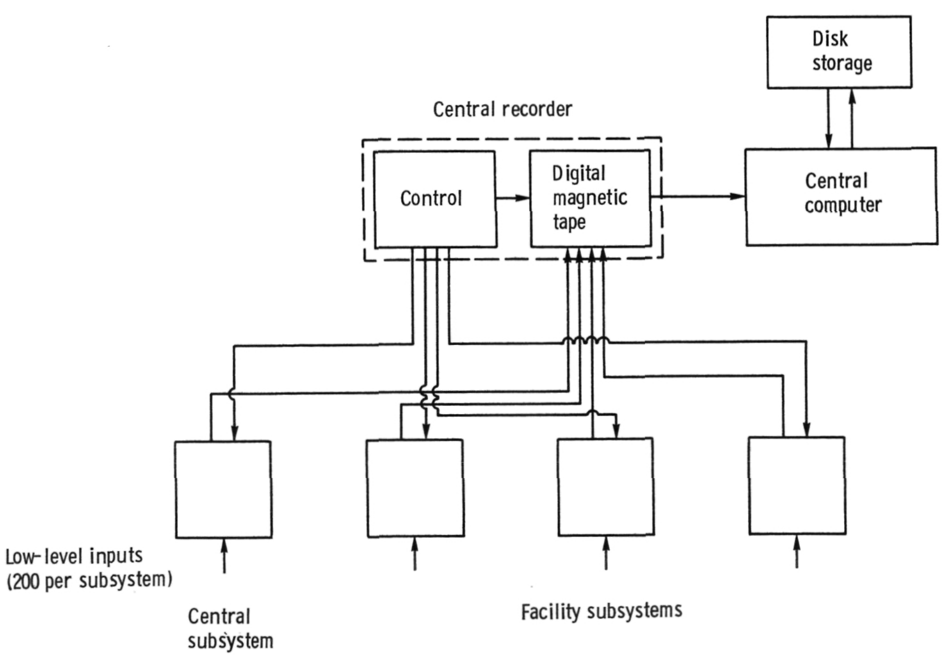

Figure 15. - TRADAR system.

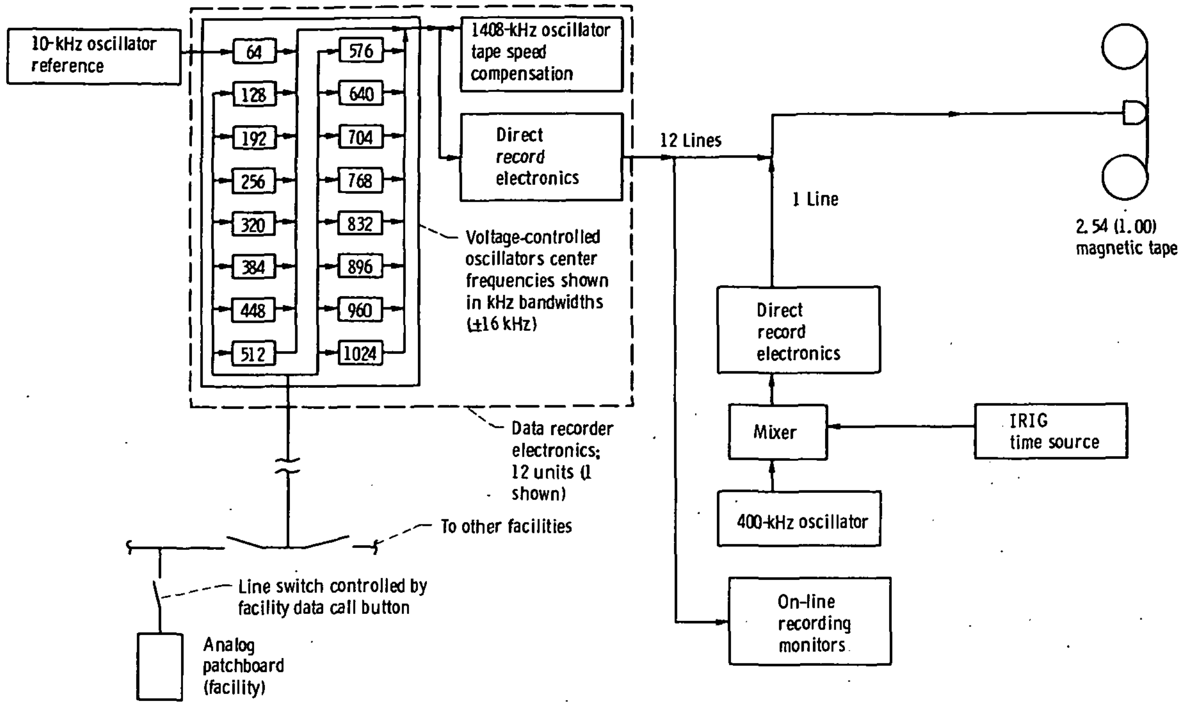

(a) Data recorder.

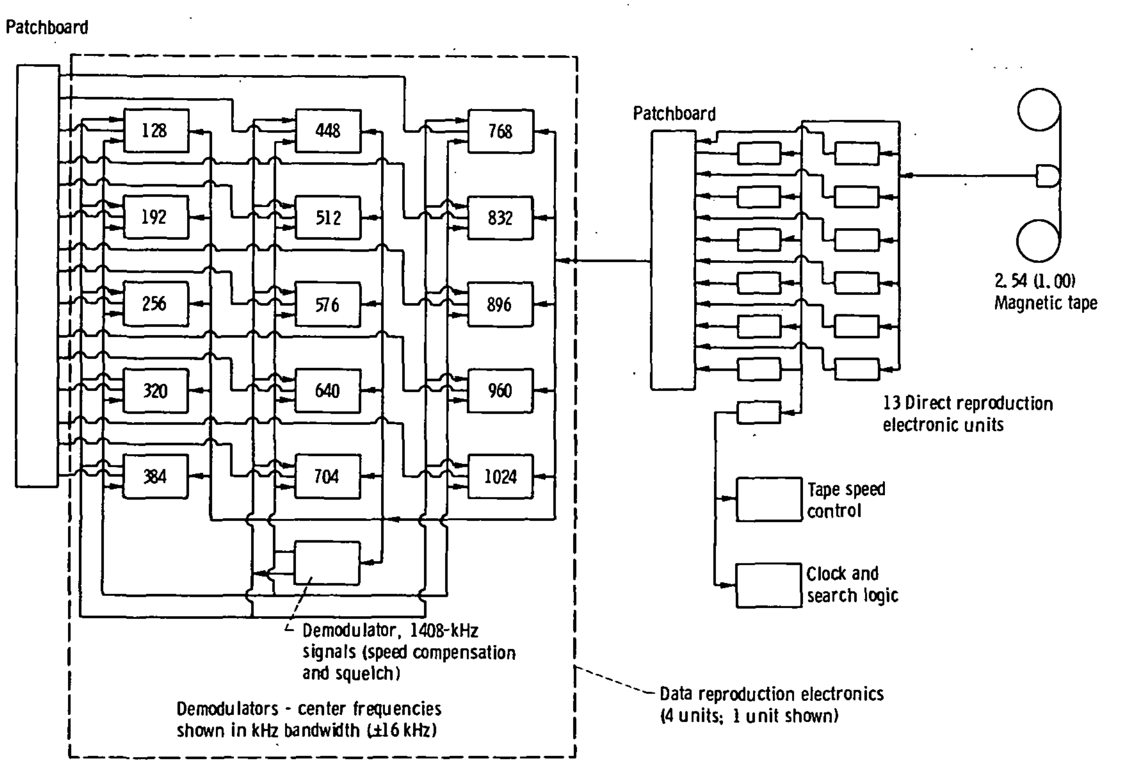

(b) Data reproduction.

Figure 16. - CARS system.

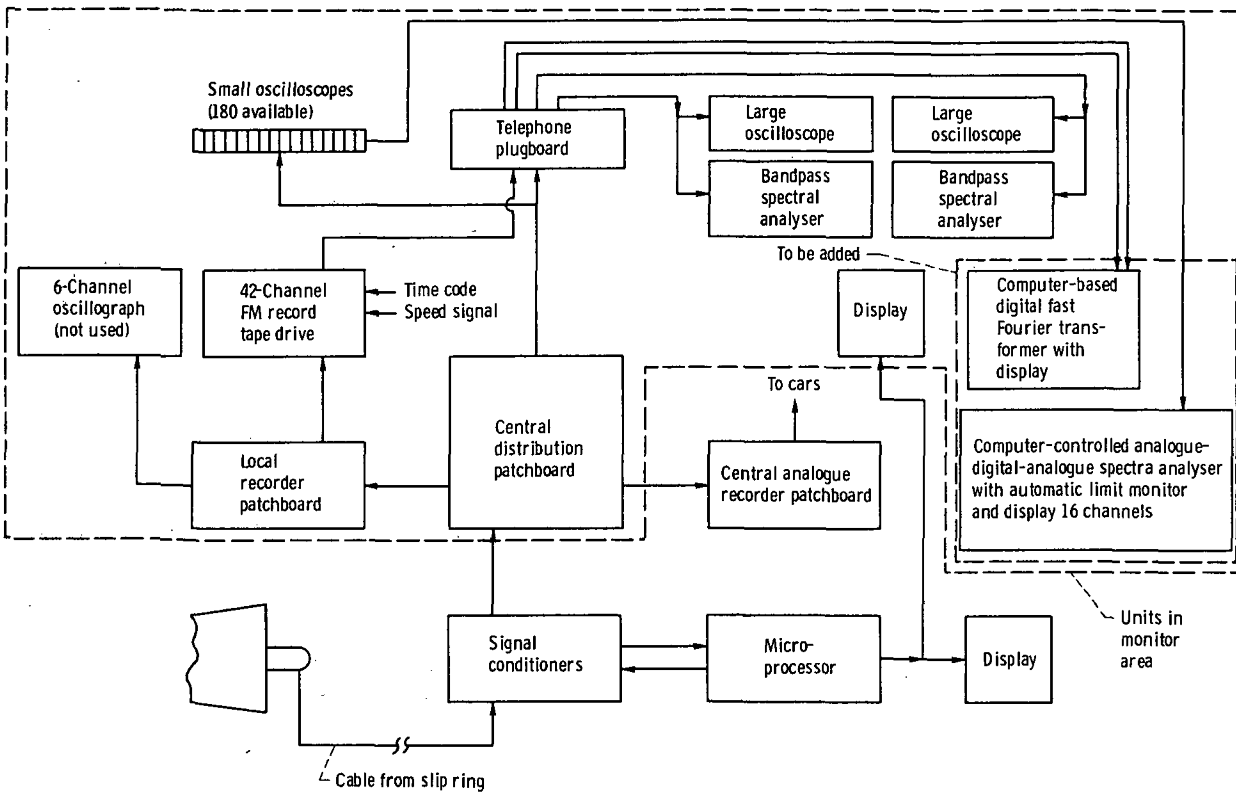

Figure 17. - Strain-gage signal distribution.

"The aeronautical and space activities of the United States shall be conducted so as to contribute . . . to the expansion of human knowledge of phenomena in the atmosphere and space. The Administration shall provide for the widest practicable and appropriate dissemination of information concerning its activities and the results thereof."

—NATIONAL AERONAUTICS AND SPACE ACT OF 1958

NASA SCIENTIFIC AND TECHNICAL PUBLICATIONS

TECHNICAL REPORTS: Scientific and technical information considered important, complete, and a lasting contribution to existing knowledge.

TECHNICAL NOTES: Information less broad in scope but nevertheless of importance as a contribution to existing knowledge.

TECHNICAL MEMORANDUMS: Information receiving limited distribution because of preliminary data, security classification, or other reasons. Also includes conference proceedings with either limited or unlimited distribution.

CONTRACTOR REPORTS: Scientific and technical information generated under a NASA contract or grant and considered an important contribution to existing knowledge.

TECHNICAL TRANSLATIONS: Information published in a foreign language considered to merit NASA distribution in English.

SPECIAL PUBLICATIONS: Information derived from or of value to NASA activities. Publications include final reports of major projects, monographs, data compilations, handbooks, sourcebooks, and special bibliographies.

TECHNOLOGY UTILIZATION PUBLICATIONS: Information on technology used by NASA that may be of particular interest in commercial and other non-aerospace applications. Publications include Tech Briefs, Technology Utilization Reports and Technology Surveys.

Details on the availability of these publications may be obtained from:

SCIENTIFIC AND TECHNICAL INFORMATION OFFICE

NATIONAL AERONAUTICS AND SPACE ADMINISTRATION

Washington, D.C. 20546